Chemical Methodologies 6(2022) 428-437

Chemical Methodologies

Journal homepage: http://chemmethod.com

*Original Research Article*

# Synthesis of Advanced ZTA for Orthopedic Application by Sol-Gel Method

**Alaa S. Taeh*, Alaa A. Abdul-Hamead, Farhad M. Othman**

*Department Materials Engineering, University of Technology, Baghdad, Iraq*

**ARTICLE INFO**

**Article history**

Submitted: 2022-03-14
Revised: 2022-04-06
Accepted: 2022-04-08
Manuscript ID: CHEMM-2203-1455
Checked for Plagiarism: **Yes**
Language Editor:
Dr. Fatimah Ramezani
Editor who approved publication:
Dr. Hassan Karimi-Maleh
**DOI**:10.22034/CHEMM.2022.334143.1455

**KEYWORDS**

ZTA
Biolox
Orthopedic
Sol-gel
Composite
SEM
XRD

**ABSTRACT**

The demand for ceramic products for orthopedic applications is increasing due to the lowest rate of wear. A fourth-generation ceramic (BIOLOX delta; CeramTec.) consists of 82 wt. % $Al_2O_3$, 17 wt. % (1.3 Yttria Stabilized $ZrO_2$), 0.5 wt. % strontium oxide, and 0.5 wt. % chromium oxide. It has good mechanical properties compared to the other generations of ceramics (BIOLOX forte and pure alumina), which may increase the range of movement and decrease the rate of dislocation. This ceramic composite (delta) has a smaller grain size (0.6 µm) than previous alumina composites (1.8 µm). So, this paper tries to obtain the smallest grain size on the scale of nanometers to improve biolox properties and good distribution for its components. By the sol-gel method, the BIOLOX delta was prepared from the gel precursor and sintering at 1100 °C for 2 h in the oven. The heat-up rate was 5 °C/min. As-obtained particles were characterized before and after sintering temperature using X-Ray Diffraction (XRD), Energy Dispersive X-Ray Analysis (EDX), and Scanning Electron Microscopy (SEM). The dried powder which was obtained consists of phases, γ-$Al_2O_3$, θ-$Al_2O_3$, and δ-$Al_2O_3$, while $ZrO_2$ is found as (t + m) $ZrO_2$ after calcination and the obtained average grain size was (10.94 nm).

**GRAPHICAL ABSTRACT**

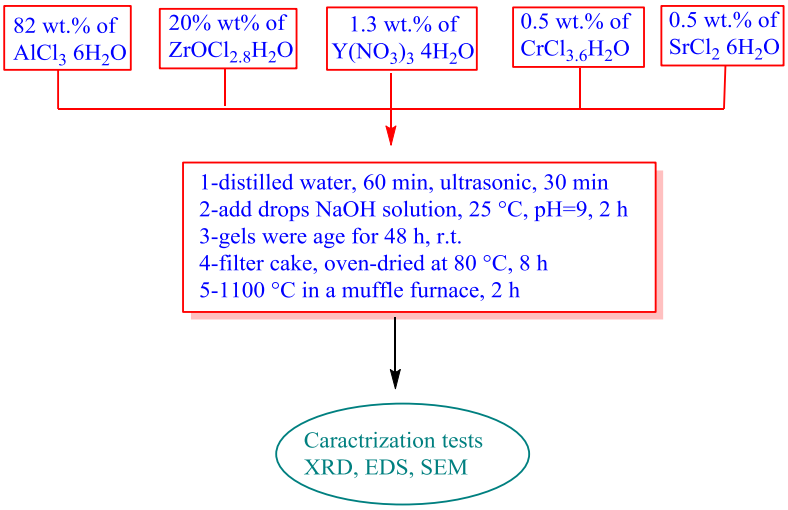


* Corresponding author: Alaa S. Taeh
✉ E-mail: alaataeh@uowasit.edu.iq

## Introduction

A top priority in modern materials technology is the development of materials that improve the quality of active human life, while also extending the duration of that life. Ceramic materials, as opposed to metals and polymers, are more biologically compatible with human body tissues and as a result, they are in high demand in medical practice [1].

Investigations are being carried out on oxide monophasic ceramics based on corundum ($Al_2O_3$) and solid solutions containing the tetragonal modification T-$ZrO_2$ (TZP). This technique is used in the surgical treatment of injuries, spine abnormalities, orthotropic illnesses, and dental restorations, among other applications.

In general, the biological response to their existence is low; they do not activate adverse immunological responses and are not rejected by the body because they are alien bodies, as is the situation with bacteria [2-3].

Zirconia Toughened Alumina (ZTA) composites have been extensively researched in terms of alumina - rich compositions (alumina in the range of 60–95% vol.). ZTA became accessible as a femoral head material in June 2000, commercialized by CeramTec. AG (Plochingen, Germany) under the trademark BIOLOX® delta. After FDA clearance in 2003, ZTA became widely utilized in THA: in the previous ten years, nearly one million CeramTec ZTA femoral heads and over 700,000 inserts have been implanted globally [2].

The characteristics of the major compounds, alumina and zirconia, alumina's hardness, corrosion resistance and biocompatibility distinguish it from the other materials. Pure alumina components have a favorable wear behavior. If you compare ceramic wear debris to metal or polyethylene particles in vivo, you will notice that it causes a less inflammatory or granulomatous reaction. Improvements have been made to $Al_2O_3$ for hip joints in the past, for example, by the use of raw materials of a better quality, enhanced production, as well as quality assurance, all of these factors have contributed to a considerable decrease in the risk of hip joint fracture. However, alumina's strength is usually restricted to 650 MPa (depending on ISO 6474-1) [4].

A 1.3 mole% Yttria concentration in tetragonal zirconia polycrystalline makes it the strongest ceramic material. Phase transformation toughening converts the metastable tetragonal phase into the stable monoclinic phase under high mechanical tensile stresses. Ceramic component strength and defect tolerance are enhanced due to the increased volume induced by phase transition. There are two major distinctions between zirconia and alumina in biological applications [5].

First, Zirconia is much tougher than non-ceramic materials. Although it has a low hardness (about 13 GPa vs. 20 GPa), 13 GPa is still tougher than non-ceramic materials used in hip implant components. Second, in a bodily fluid environment, zirconia's metastable tetragonal phase transitions slowly. That is also known as Low-Temperature Degradation (LTD) or hydrothermal aging. Under certain conditions, hydrothermal aging may degrade the surface strength and quality of pure zirconia items. It is one of the reasons why TZP is no longer often used in medical bearing applications, despite the fact that it is an extensively used material in dental applications [6-7].

When combined with zirconia's toughening action, alumina's outstanding hardness and stability result in ZTA materials with the exceptional toughness and stability. Alumina percentages of 60–90 weight percent and a zirconia content of 10–30 weight percent are recommended by the ISO standard 6474-2 for ZTA composites used in medical applications. Zirconia has a greater density than alumina (3.99 g/$cm^3$, compared to 6.09 g/$cm^3$) and hence, it has a larger volume share in the ceramic industry. The most extensively used ZTA material, BIOLOX® delta from Ceram Tec in Germany, is composed of 80% $AL_2O_3$, 17% $ZrO_2$, and 3% ($SrAl_{12}$–x$CrxO_{19}$) strontium aluminate platelets. Alumina is the most common component of ZTA materials. Because of this low concentration, individual zirconia grains are largely segregated from one another at this low concentration. Individual zirconia grains are spared from the effects of hydrothermal aging as a consequence of this. The alumina matrix which

surrounds the area effectively stops further spread. A previous study proved the material's good stability under rapid aging conditions, 5–10 times the expected lifespan of the implant [8]. The composite's low zirconia content improves strength and hardness compared to alumina pure. The average strength is 1380 MPa; more than double that of pure alumina. The fracture toughness has increased by 50% to 6 MPa $m^{1/2}$. Hardness is lost compared to the pure alumina. As a softener, a little amount of chromium oxide ($Cr_2O_3$) was added to compensate for the loss of zirconia. Finally, during the sintering process, strontium oxide (SrO) applied to the material creates strontium aluminate ($SrAl_{12}$–$xCrxO_{19}$) platelets. These flat, elongated crystals, because of their size, prevent cracks from expanding by dispersing crack energy. In reality, when the crack reaches one of these crystals, it requires more energy to move around it; otherwise, the crack does not grow. The finished product contains around 82% alumina, 17% zirconia, and less than 2% chromium oxide and strontium oxide [2, 8, 9]. However, although the composite's hardness is highly connected to the major material components which make up the composite, this isn't the only factor that influences its hardness. As a result, under the assumption of continuous processing, compared to pure alumina, zirconia reduces the hardness of the finished material [7].

The ceramic composite fabrication is separated into several steps. The ceramic composite powder is initially prepared using several processes such as mixing mechanically, the sol gel process, hydrothermal oxidation, and so on. Green powder production is the second stage, which may be performed using a number of procedures such as wet pressing, die pressing, cold isostatic pressing, and uniaxial pressing in order to produce green compressed bodies. Finally, the green compressed powders make them denser through a sintering process.[5].

The homogeneous distribution of $ZrO_2$ in the ceramic matrix is important for maximizing the toughening caused by micro cracks. The uniform dispersion of zirconia particles in the alumina matrix may be controlled via homogeneous powder production processes. A range of powder processing procedures have been developed to produce homogenous powder mixes, with precipitation and sol–gel processes being the most simple and commercialized chemical synthesis strategies for producing zirconia doped nanoparticles [11].

The manufacture of $ZrO_2$ dispersed $Al_2O_3$ precursor powders from multiphase hydrogel is a complicated process which is dependent on the configuration of Al and Zr hydroxide and its polymerization.

Acid/base characteristics affect the polymerization and chemistry of aluminum oxides and hydroxides. The oxygen coordination surrounding $Al^{3+}$ has a substantial impact on proton activity. In water, the aluminum hydroxide $Al(OH)_4$ was a deprotonated form, which contains tetrahedrally coupled Al atoms with oxygen atoms, while all of the cationic forms with protonation in the chain have Al atoms that are tetrahedrally coordinated with oxygen atoms $Al(OH)_2$+(aq) to $Al_3$+(aq) are six-coordinated. The hydrogel's stability is due to the amphoteric properties of $Al(OH)_3$ in water [12-13].

The aim of this paper was to fabricate ZTA like BIOLOX delta using the sol gel method and investigate the characterization properties and effect of sintering temperature on component phases.

## Materials and Methods

BIOLOX delta is produced using a chemical process which uses alumina precursors, zirconia, Yttria, strontium, and chromium utilizing the sol - gel method. 82 wt.% of aluminum chloride ($AlCl_3$ $6H_2O$, from Sigma-Aldrich) was hydrolyzed in distilled water, separately, a 20% wt% of partly stabilized zirconia was synthesized by hydrolysis of zirconyl chloride octahydrate ($ZrOCl_2.8H_2O$ from Sigma-Aldrich) with the 1.3 wt.% yttrium(III) nitrate tetrahydrate ($Y(NO_3)_3$ $4H_2O$ from Sigma-Aldrich), then was mixed with precursors of alumina. 0.5 wt.% of chromium (III) chloride hexahydrate ($CrCl_3.6H_2O$ from Sigma-Aldrich) and 0.5 wt.% of strontium chloride hexahydrate ($SrCl_2$ $6H_2O$ from Sigma-Aldrich) also were hydrolyzed in distilled water, for 60 min in

ultrasonic machine followed by automatic stirrer for 30 min.

Strontium and chromium precursors were added to hydrolyze zirconium and aluminum mixtures. The ingredients were thoroughly stirred together. By adding a drop-by-drop ratio of a 1:1 NaOH solution to a continually stirred mixture of Al and Zr salts kept at a temperature of 25 °C, the mixed hydrogel was formed. The batch's viscosity slowly grew until it reached a pH of 9, which resulted in an unblocked gel. After that, the gels were allowed to age for 48 hours at room temperature. Following that, to eliminate chloride and nitrate ions from the gels of each composition, they were repeatedly washed with boiling distilled water, and then they were filtered to remove any remaining ions. The filter cake was oven-dried at 80 °C for 8 hours. At 1100 °C in a muffle furnace, some of the dry gels were calcined in the air at a heat-up rate of 5 °C/min for a total holding period of 2 hours at the respective peak temperatures, then left to cool inside the furnace. The composition steps are as shown in Figure 1.

The calcined powders and dried gel were subjected to X-ray diffraction examinations in a Philips X-ray diffractometer (Model: XRD-6000), which used Cu radiation, in order to determine their phase composition. The voltage and current settings were 40 kV and 30 mA, respectively and the voltage and current were measured.

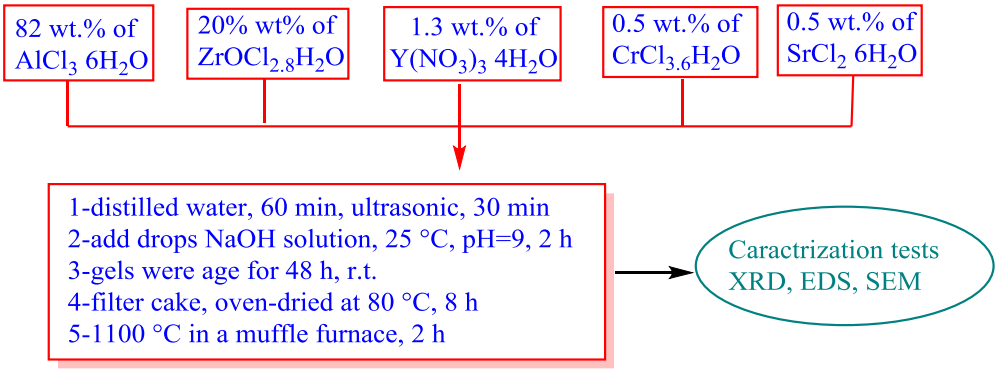


**Figure 1:** The flowchart of fabrication steps for BIOLOX

The samples were scanned continuously with a step size of 0.2 degrees and a count time of 1.20 s for each step, with the step size being 0.2 degrees. Silicon was employed as an internal standard throughout the project. From X-ray line broadening and Scherrer's equation, it was possible to calculate the average grain size (D) (nm) for the produced powder [14].

$$D = \frac{0.94\lambda}{[\Delta_{2\theta} \cos\theta]} \quad (1)$$

In which, **D** is the crystallite size (nm)

λ: is the x-ray wavelength (1.54056 °A).

$\Delta_{2\theta}$: FWHM; is the Full Width at Half Maximum (radian).

θ: is the Bragg diffraction angle of the XRD peak (degree).

For a certain crystal plane (hkl) in a polycrystalline film, the orientation was preferred [15]:

$$T_C = \left( \frac{I_{hkl} / I_{\circ hkl}}{M^{-1} \sum \frac{I_{hkl}}{I_{\circ hkl}}} \right) \quad (2)$$

In which,

$T_C$: is the texture coefficient for a certain (hkl) plane.

I': is the measured intensity value.

$I_o$: is the COD standard intensity value of the corresponding powder.

M: is the number of reflections observed in the XRD trace.

In the sample, the dislocation density (δ\) has been obtained by using the equation [14]:

$$\rho = \frac{1}{D^2} \quad (3)$$

Where, ρ: is the dislocation density. The structural result from XRD data of ZTA powders is in Tables (1,2).

The microstructure of powders was examined using a scanning electron microscope (carried out by an electron gun tungsten, secondary electron detector mode, ultrahigh vacuum ($10^{-6}$ mbar), 20 kV of accelerating voltage, and variable working distance, SEM MAG was 10.0KX, (Type TESCAN VEGA III) (CZECH)), coupled with an energy dispersion spectroscopy (EDS) equipment with a voltage of up to 20 kV and magnifications up to 50 kX was used for examination of the precursor materials and the functionalized final product.

## Results and Discussion

*X-Ray Diffraction Results*

The XRD analysis of the hydrogel was performed. As depicted in figure 2a, the XRD pattern of the as-dried gel at 80 ºC exhibits a large peak of bayerite ($Al(OH)_3$), which corresponds to COD (Crystallography Open Database) 96-900-8136 (bayerite) [16]. The broad peak of bayerite represented the existence of fine crystallites (crystallite size15.65 nm). Also the hydrogel confirms the existence of monoclinic zirconium oxide $ZrO_2$ (COD 96-900-7449 and 96-230-0204) [14],[15], the amorphous intermediate boehmite, Sr-OH (COD 96-210-0156) [19], and Cr-O (COD 96-901-5443) [20] bond (Table 1).

A higher temperature of 1100 °C causes more phase transitions in boehmite and also the crystallization of zirconia from amorphous zirconium oxide when the material is calcined at a greater rate (Fig. 2b). At this temperature, the different phases were seen to present m-$ZrO_2$, t-$ZrO_2$ according to COD (96-900-7486,96-152-5707, and 96-230-0613, respectively) [18–20], and δ-$Al_2O_3$, θ-$Al_2O_3$ and γ-$Al_2O_3$ according to COD (96-154-4375, 96-120-0006, and 96-101-0462, respectively) [21-23], as well as to ceria (SrO) according to COD (96-101-1329) [27] , chromium oxide ($Cr_2O_3$) according to COD (96-901-6610)[28] and $Al_{12}Cr_2O_{32}Sr_8$ according to COD (96-810-3787) [29]. At 1100 °C for 2 hours, the crystallite size of the calcined powders is in the range of 10.94 nm. α-$Al_2O_3$ generally crystallizes at temperatures nearly 1100 °C due to its small crystallite size and large specific surface area. However, in the current investigation, crystallization of α-$Al_2O_3$ was inhibited due to the presence of additional oxide additions in the solution [11].

The comparison of XRDs indicates a higher degree of crystallinity of the heat-treated sample at 1100 ºC, while the phase transformation for α-$Al_2O_3$ is detected but not completely, also that for $ZrO_2$ tetragonal phases are not completely transformation. That was because of impurities or the sintering temperature was not enough [30].

**Table 1**: Results data of XRD before sintering

| Compund | Phase | $2\theta_m$ dgree | hkl | FWHM | D (nm) | $T_c$ | ρ $10^{-21}$ ($m^{-2}$) |
|---|---|---|---|---|---|---|---|
| $ZrO_2$ | Monoclinic | 40.579 | 21-1 | 0.5703 | 17.26 | 1.15795891 | 3.35675 |
| | | 57.496 | -131 | 0.49630 | 19.08 | 0.25804918 | 2.7469 |
| | | 59.32 | -131 | 0.6325 | 15.10 | 0.23945955 | 4.38577 |
| | | 70.61 | 32-2 | 0.6886 | 14.77 | 0.84453236 | 4.58394 |
| $Al(OH)_3$ Bayerite | Monoclinic | 18.79 | 001 | 0.5250 | 16.03 | 0.14716707 | 3.89164 |
| | | 20.33 | 110 | 0.53380 | 15.80 | 0.22479806 | 4.00577 |
| | | 27.85 | 111 | 0.61110 | 13.99 | 0.42498845 | 5.10934 |
| | | 33.18 | -121 | 1.40000 | 6.19 | 0.37288954 | 2.60987 |
| | | 53.17 | -132 | 0.56860 | 16.33 | 0.33959926 | 3.74997 |
| | | 63.62 | 330 | 0.36300 | 26.91 | 0.15722429 | 1.38093 |
| $Y_2O_3$ | Cubic | 20.33 | 211 | 0.53380 | 15.80 | 2.86932054 | 4.00577 |
| | | 57.496 | 622 | 0.49630 | 19.08 | 0.04192197 | 2.7469 |
| | | 70.61 | 800 | 0.6886 | 14.77 | 0.42209083 | 4.58394 |
| $Cr_2O_3$ | Trigonal (hexagonal axes) | 53.17 | 204 | 0.56860 | 16.33 | 10 | 3.74997 |
| $SrO_{10}H_{18}$ | Tetragonal | 55.71 | 226 | 0.77260 | 12.15 | 0.36706127 | 6.77404 |
| | | 30.64 | 004 | 1.96360 | 4.38 | 0.9514047 | 5.21257 |
| | | 70.61 | 064 | 0.6886 | 14.77 | 2.01486736 | 4.58394 |

**Table 2:** Results data of XRD after sintering

| Compound | Phase | $2\theta_m$ dgree | hkl | FWHM | D (nm) | $T_c$ | $\rho\ 10^{-21}$ ($m^{-2}$) |
|---|---|---|---|---|---|---|---|
| $ZrO_2$ | Tetragonal | 30.28 | 101 | 0.76820 | 11.19 | 0.24180036 | 7.98619 |
| | | 35.06 | 110 | 1.23260 | 7.06 | 0.29498886 | 20.0628 |
| | | 60.22 | 211 | 0.70400 | 13.63 | 0.30009896 | 5.3828 |
| | | 62.80 | 202 | 0.75000 | 12.97 | 0.25954252 | 5.94456 |
| | | 74.48 | 220 | 0.88810 | 11.74 | 0.27295638 | 7.25544 |
| | | 81.62 | 213 | 0.80000 | 13.71 | 0.2972796 | 5.32016 |
| | Monoclinic | 35.06 | 200 | 1.23260 | 7.06 | 1.14238776 | 20.0628 |
| | | 50.3837 | -122 | 1.04450 | 8.78 | 3.85761224 | 12.9721 |
| $Al_2O_3$ | Theta monoclinic | 62.80 | 80-1 | 0.75000 | 12.97 | 1.81804679 | 5.94456 |
| | | 83.6176 | 620 | 0.00000 | | 3.18195321 | |
| | Gamma cubic | 39.4929 | 111 | 0.84250 | 10.47 | 4.45357487 | 9.12235 |
| | | 45.8303 | 200 | 1.44000 | 6.26 | 0.5464257 | 25.5183 |
| | Delta orthorhombic | 35.0615 | 020 | 1.23260 | 7.06 | 2.83431921 | 20.0628 |
| | | 39.4929 | 120 | 0.84250 | 10.47 | 0.03770305 | 9.12235 |
| | | 50.3837 | 220 | 1.04450 | 8.78 | 0.4613105 | 12.9721 |
| $Y_2O_3$ | Cubic | 60.2243 | 444 | 0.70400 | 13.63 | 1.01708056 | 5.3828 |
| | | 74.4840 | 563 | 0.88810 | 11.74 | 0.39076712 | 7.25544 |
| | | 83.6176 | 842 | 0.00000 | | 0.63815213 | |
| | | 95.2975 | 1002 | 1.05930 | 11.64 | 0.45400018 | 7.38064 |
| $Cr_2O_3$ | Trigonal (hexagonal axes) | 50.3837 | 204 | 1.04450 | 8.78 | 2.97722097 | 12.9721 |
| | | 95.2975 | 2110 | 1.05930 | 11.64 | 2.02277903 | 7.38064 |
| SrO | Cubic | 30.2766 | 111 | 0.76820 | 11.19 | 0.99531269 | 7.98619 |
| | | 50.3837 | 202 | 1.04450 | 8.78 | 0.67135397 | 1.29721 |
| | | 95.2975 | 422 | 1.05930 | 11.64 | 1.66666667 | 7.38064 |
| $Al_{12}Cr_2O_{32}Sr_8$ | Orthorhombic | 32.8400 | 240 | 0.64000 | 13.52 | 10 | 5.47075 |

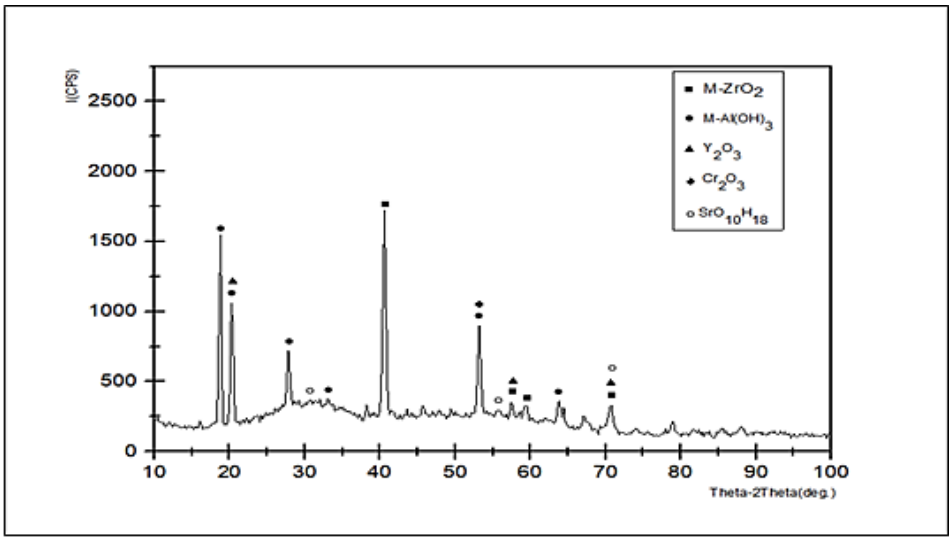


(a)

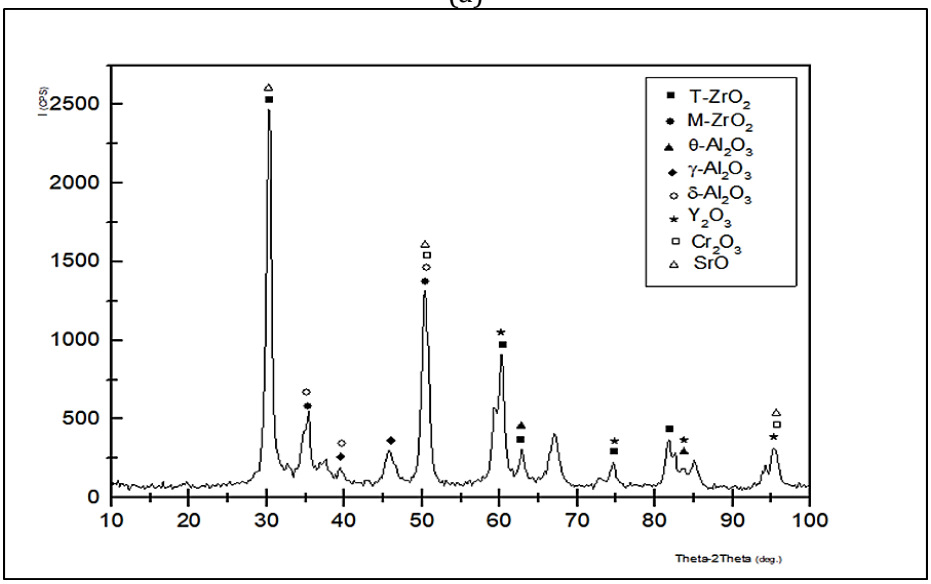


(b)

**Figure 2:** The XRD patterns of biolox powders a) before b) after sintering at 1200 ºC

*Energy Dispersive X-Ray Analysis Results*

Energy-dispersive X-ray spectroscopy (EDS) of the Biolox prepared specimens consisting of 80 vol. % of $Al_2O_3$ matrix and 17 vol. % of $ZrO_2$ is illustrated in figs. 3 & 4.

Following the sintering temperature of 1100 ºC, as indicated in fig. 4, it was discovered that there was a maximum amount of Al element of 28.56 wt. % and a minimum value of Zr element of 9.61 wt.% in the sintered samples of the composite. As displayed in fig. 3, the highest value of the Al element was 26 wt. % and the lowest value of the Zr element was 3.75 wt. % when no sintered composite samples were used, as compared to the sintered samples of the composite. We know that alumina is a hard substance and that zirconia is a tough material, so we'll stick with that.

Alumina has a harder surface than zirconia, which is a good thing. Accordingly, the increased values of the $Al_2O_3$ and $ZrO_2$ elements discovered in the composites suggest an enhancement of the hardness and fracture toughness of the composites. Based on fig. [2b], this might be referred to the stress-induced martensitic transition of stable dioxide (t-$ZrO_2$) to manganese dioxide (m-$ZrO_2$) which occurred in the stress field around a spreading fracture, which increased the toughness of zirconia ceramics. When compared to composite samples which were not sintering, the biolox-sintered sample with a higher weight percent of aluminum demonstrated superior tribological behavior.

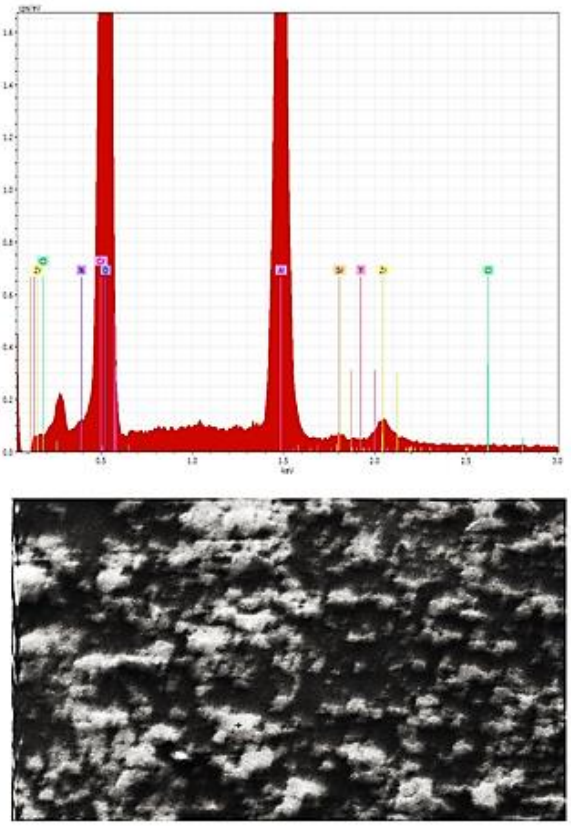

Spectrum: Acquisition 3875

| El | AN | Series | unn. C [wt.%] | norm. C [wt.%] | Atom. C [at.%] | Error (1 Sigma) [wt.%] |
|---|---|---|---|---|---|---|
| O | 8 | K-series | 42.35 | 42.09 | 8.91 | 4.99 |
| H | 1 | K-series | 26.22 | 26.06 | 87.53 | 2.65 |
| Al | 13 | K-series | 26.16 | 26.00 | 3.26 | 1.29 |
| Zr | 40 | L-series | 3.77 | 3.75 | 0.14 | 0.25 |
| Cr | 24 | L-series | 1.08 | 1.08 | 0.07 | 0.35 |
| Sr | 38 | L-series | 0.49 | 0.48 | 0.02 | 0.07 |
| Y | 39 | L-series | 0.26 | 0.26 | 0.01 | 0.06 |
| N | 7 | K-series | 0.23 | 0.23 | 0.06 | 0.11 |
| Cl | 17 | K-series | 0.05 | 0.05 | 0.00 | 0.04 |
| | | Total: | 100.63 | 100.00 | 100.00 | |

**Figure 3:** EDXS test for bolox before sintering

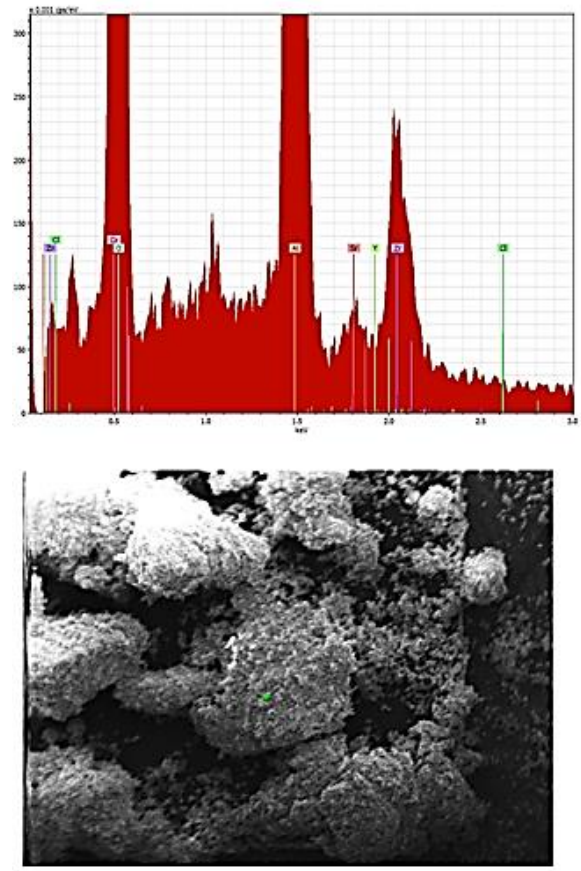

| El | AN | Series | unn. C [wt.%] | norm. C [wt.%] | Atom. C [at.%] | Error (1 Sigma) [wt.%] |
|---|---|---|---|---|---|---|
| H | 1 | K-series | 30.55 | 32.14 | 91.71 | 3.08 |
| Al | 13 | K-series | 27.15 | 28.56 | 3.04 | 1.51 |
| O | 8 | K-series | 25.39 | 26.71 | 4.80 | 4.52 |
| Zr | 40 | L-series | 9.13 | 9.61 | 0.30 | 0.82 |
| Cr | 24 | L-series | 1.69 | 1.77 | 0.10 | 1.09 |
| Y | 39 | L-series | 0.57 | 0.60 | 0.02 | 0.16 |
| Sr | 38 | L-series | 0.57 | 0.60 | 0.02 | 0.16 |
| Cl | 17 | K-series | 0.00 | 0.00 | 0.00 | 0.00 |
| | | Total: | 95.04 | 100.00 | 100.00 | |

**Figure 4:** EDXS test for bolox after sintering

## Conclusion

The following are the primary findings that might be taken from the current investigation:

- When compared to the microstructure properties of sintering-created composite samples, the microstructure properties of sintering-created samples were greatly improved. When compared to un-sintered samples, the sintered composite may have encouraged a higher degree of crystallization in the elements, resulting in improved material characteristics.
- When $ZrO_2$ transformation toughening is present in a composite sample, XRD examination reveals that the monoclinic phase is decreased and the tetragonal phase is enhanced, resulting in better fracture toughness of that composite sample. However, the sintering temperature of 110 ºC is too low for achieving alumina phase change and obtaining a α -phase that is suitable for medical applications [28,29]. Additionally, improvements in the surface roughness and crystallization of the material have been observed, as demonstrated in the accompanying figures.

## Acknowledgments

*My thanks and gratitude to everyone who continuous support and review of all work. I also extend my thanks and gratitude to everyone who participated in his research and work in the service of society.*

**ORCID:**
Alaa S. Taeh
*https://www.orcid.org/0000-0003-0131-2973*

## References

[1]. Rahaman M.N., Yao A., Bal B.S., Garino J.P., Ries M.D., *J. Am. Ceram. Soc.*, 2007, **90**:1965, [Crossref], [Google Scholar], [Publisher]
[2]. Palmero P., Montanaro L., Reveron H., Chevalier J., *Materials*, 2014, **7**:5012 [Crossref], [Google Scholar], [Publisher]
[3]. Podzorova L.I., Il'icheva A.A., Pen'kova O.I., Alad'ev N.A., Volchenkova V.A., Kutsev S.V., Shvorneva L.I., *Inorg. Mater. Appl. Res.,* 2016, **7**:724 [Crossref], [Google Scholar], [Publisher]
[4]. Deville S., Chevalier J., Dauvergne C., Fantozzi G., Bartolomé J.F., Moya J.S., Torrecillas R., *J. Am. Ceram. Soc.*, 2005, **88**:1273 [Crossref], [Google Scholar], [Publisher]
[5]. Gopal V., Manivasagam G., *Appl. Nanocompos. Mater. Orthopedics,* 2019, 201 [Crossref], [Google Scholar], [Publisher]
[6]. Sivanesan S., Loong T.H., Namasivayam S., Fouladi M.H., *Key Eng. Mater.,* 2019, **814**:12 [Crossref], [Google Scholar], [Publisher]
[7]. Kuntz M., Krüger R., *Ceram. Int.*, 2018, **44**:2011 [Crossref], [Google Scholar], [Publisher]
[8]. Kuntz M., Krüger R., *Ceram. Int.*, 2020, **44**:2011 [Crossref], [Google Scholar], [Publisher]
[9]. Affatato S., Modena E., Toni A., Taddei P., *J. Mech. Behav. Biomed. Mater.*, 2012, **13**:118 [Crossref], [Google Scholar], [Publisher]
[10]. Kuntz M., Masson B., Pandorf T., *Strength Mater.*, 2009, 133–155, [Google Scholar], [Publisher]
[11]. Sarkar D., Mohapatra D., Ray S., Bhattacharyya S., Adak S., Mitra N., 2007, **33**:1275 [Crossref], [Google Scholar], [Publisher]
[12]. Catauro M., Vecchio Ciprioti S., *Sol-gel synthesis and characterization of hybrid materials for biomedical applications*. In *Thermodynamics and Biophysics of Biomedical Nanosystems* (pp. 445-475). Springer, Singapore. 2019 [Crossref], [Google Scholar], [Publisher]
[13]. D. Sarkar, D. Mohapatra, S. Ray, S. Bhattacharyya, S. Adak, N. Mitra, *Ceram. Int.*, 2007, **33**:1275 [Crossref], [Google Scholar], [Publisher]
[14]. Abdullah-Hamead A.A., *Mater. Sci. Forum*, 2020, **1002**:319 [Crossref], [Google Scholar], [Publisher]
[15]. Abdul-Hamead A.A., Othman F.M., Fakhri M.A., *J. Mater. Sci. Mater. Electron.*, 2021, **32**:15523 [Crossref], [Google Scholar], [Publisher]
[16]. Rothbauer R., Zigan F., O'Daniel H., *Z. Kristallogr. Cryst. Mater.*, 1967, **125**:317 [Crossref], [Google Scholar], [Publisher]
[17]. Wood I.G., Vocadlo L., Dobson D.P., Price G.D., Fortes A.D., Cooper F.J., Neale J.W., Walker A.M., Marshall W.G., Tucker M.G., Francis D.J., Stone H.J., McCammon C.A., *J. Appl. Cryst.*, 2008, **41**:886 [Crossref], [Google Scholar], [Publisher]
[18]. McCullough J.D., Trueblood K.N., *Acta Cryst*, 1959, **12**:507 [Crossref], [Google Scholar], [Publisher]

[19]. Ricci J.S., Stevens R.C., McMullan R.K., *Acta Cryst. B*, 2005, **61**:381 [Crossref], [Google Scholar], [Publisher]
[20]. Kantor A., Kantor I., Merlini M., Glazyrin K., Prescher C., Hanfland M., *Am. Mineral.*, 2012, **97**:1764 [Crossref], [Google Scholar], [Publisher]
[21]. Smith D.K., Newkrik W., Acta Crystallogr. 1965, **18**:983 [Crossref], [Google Scholar], [Publisher]
[22]. Bouvier P., Djurado E., Lucazeau G., *Phys. Rev. Ser.*, 2000, **62**:8731 [Crossref], [Google Scholar], [Publisher]
[23]. Lutterotti L., Scardi P., *J. Appl. Cryst.*, 1990, **23**:246 [Crossref], [Google Scholar], [Publisher]
[24]. K. Y. Komatsu K., Sano A., Momma K., Ohtani E., *Z. Kristallogr.*, 2007, **222**:13 [Crossref], [Google Scholar], [Publisher]
[25]. Husson E., Repelin Y., *Eur. J. Solid State Inorg. Chem.*, 1996, **33**:1223 [Crossref], [Google Scholar], [Publisher]
[26]. Verwey E.J.W., *Z. Kristallogr. Cryst. Mater.*, 1935, **91**:317 [Crossref], [Google Scholar], [Publisher]
[27]. Gerlach W., *Z. Physik.*, 1922, **9**:184 [Crossref], [Google Scholar], [Publisher]
[28]. H. R. M. Finger L. W., *J. Appl. Phys.*, 1980, **51**:5362 [Crossref], [Google Scholar], [Publisher]
[29]. Többens D.M., Depmeier W., *Z. Krist.*, 2001, **216**:586 [Crossref], [Google Scholar], [Publisher]
[30]. Piconi C., Maccauro G., 1999, **20**:1 [Crossref], [Google Scholar], [Publisher]
[31]. Yao Z., Peng Y., Xia C., Yi X., Mao S., *J. Alloys Compd.*, 2020, **827**:154345 [Crossref], [Google Scholar], [Publisher]
[32]. Li J., Pan Y., Xiang C., *Ceram. Int.*, 2006, **32**:587 [Crossref], [Google Scholar], [Publisher]

**HOW TO CITE THIS ARTICLE**
Alaa S. Taeh, Alaa A. Abdul-Hamead, Farhad M. Othman. Synthesis of Advanced ZTA for Orthopedic Application by Sol-Gel Method. *Chem. Methodol.*, 2022, 6(6) 428-437
https://doi.org/10.22034/CHEMM.2022.334143.1455
URL: http://www.chemmethod.com/article_148106.html